Validation of genetic markers of RGC types in zebrafish

Project Report

Submitted to

Faculty of Sciences, Savitribai Phule Pune University.

Submitted By

Shriya Lele
(IBB-2013-13)

Under the guidance of Prof. Dr. Herwig Baier,
Genes-Circuits-Behavior Laboratory,
Max Planck Institute of Neurobiology

Institute of Bioinformatics and Biotechnology,

Savitribai Phule Pune University,

Pune, India

May, 2018

ACKNOWLEDGEMENTS

I would like to express my deepest gratitude to Prof. Ameeta Ravikumar for providing me with the prospect of working on my Master's thesis at a laboratory of my choice. I would like to extend this gratitude to Prof. Dr. Herwig Baier for accepting me as a Master's thesis student and offering me the opportunity to work at one of the finest laboratories in the field of neuroscience. The state-of-the-art infrastructure and the superluminal minds in the laboratory created an encouraging and inspiring platform for research.

I'm hugely indebted to Yvonne Kölsch, my supervisor and an excellent teacher, whose outstanding research launched the greater part of this thesis. Her unstinting guidance and encouragement kept me engaged in my project work, while bolstering my love for the neurosciences. I would also like to acknowledge her personal generosity which made my stay in Munich very enjoyable!

My sincerest thanks to Dr. Manuel Stemmer, Dr. Miguel Fernandes, Enrico Kühn, Irene Ammer for their help with my experiments and all the troubleshooting that came with it! I am thankful to Dr. Karin Finger-Baier for assisting me with getting proper zebrafish training and Annegret Cerny for assisting me with all the paperwork. Everyone in the Baier lab was very welcoming and friendly, which definitely made my work a very happy experience!

Finally, I would like to thank my parents and friends, for being unparalleled sources of inspiration and support. Thank you for always motivating me to put my best foot forward!

Title of the project: Validation of genetic markers of RGC types in zebrafish

Name of the student: Shriya Lele

Roll no.: IBB-2013-13

Name and designation of the guide: Prof. Dr. Herwig Baier,

Director, Max Planck Institute of Neurobiology

Duration of the project: 15.12.2017 – 25.04.2018

Keywords: cell type classification**,** retinal projectome, RNA-sequencing, genetic markers, Q-system, HITI-mediated CRISPR/Cas9 transgenesis, intersectional genetics

Abstract:

Retinal ganglion cells (RGCs) are the output neurons of the visual system and exhibit tremendous diversity in morphology. The retinal projectome offers a comprehensive classification of RGCs in zebrafish based on their dendritic stratification and axonal projections to the retinorecipient brain regions, and thus a blueprint for the physiological characterization of RGC types. Attempts at establishing a molecular atlas of RGC types using high-throughput single-cell RNA-sequencing and subsequent bioinformatic analysis revealed 41 putative points of genetic access to morphologically classified RGC types.

However, the morphological identity of RGC types defined by a molecular feature remains to be validated. We established a homology independent targeted integration-mediated CRISPR/Cas9 approach using the Q-system, to map two of the candidate markers – *barhl1b* and *eomesa* – onto morphologically classified RGC types. The Q system is a bipartite system that is analogous to the Gal4/UAS system. It comprises QF2, a transcription factor that binds to its upstream activator sequence - QUAS and drives the expression of a transgene. The RGC-type locus-specific knock-in of the transgenes enabled us to drive transient expression of a reporter which matched the endogenous expression patterns observed from *in situ* hybridizations. This transgenesis approach used in conjunction with an intersectional reporter line, allowed us to label RGC types defined by a marker gene. Both candidate markers –

barhl1b and *eomesa* – appeared to label discrete RGC types. The chemogenetic ablation tool encoded in the intersectional reporter efficiently impaired visual function as tested in a behavioral assay, thus allowing for future functional analysis of RGC types.

Taken together, a pipeline for the validation of RNA-seq identified genetic markers for RGC types was successfully established and will be used for the validation of many other candidate markers. Coupled with genetic intersectional tools, this method will allow functional investigations of RGC types.

TABLE OF CONTENTS

LIST OF TABLES AND FIGURES

LIST OF ABBREVIATIONS

AP – alkaline phosphatase

CRISPR – Clustered Regularly Interspaced Short Palindromic Repeats

Dpf – Days post fertilization

epNTR – enhanced potency nitroreductase

GFP – Green fluorescent protein

HITI – Homology independent targeted integration

MTZ - Metronidazole

PBST – Phosphate buffered saline-Tween20

PFA – Paraformaldehyde

RFP – Red fluorescent protein

RGCs – Retinal ganglion cells

WT – Wild type

CHAPTER 1: REVIEW OF LITERATURE

1.1 Need for neuronal classification

Ramón y Cajal's 100 year old manuscript - 'Histology of the Nervous System of Man and Vertebrates' is credited with being the first attempt to classify neurons. Over the last decade, neurobiologists have come to appreciate that investigating the development of the brain and elucidating its physiology and disease is bolstered by the descriptive enterprise of cell-type categorization [1]. Thousands of neurons and an even greater number of synapses, both displaying tremendous diversity contribute to the complexity of the brain. Thus, assigning morphology, genes or pathologies to certain cell-types, instead of broader regions in the brain is a crucial mode of making progress in understanding the organizing principles of brain function.

As more and more known cell-types get classified, previously unknown cell-types may emerge, perhaps even leading to the identification of molecules that may serve as markers for specific cell morphologies and physiologies. While patterns of connectivity may be mapped easily for invertebrates that possess simple neuronal circuitry, studies conducted in vertebrates with different methods, in different places and at different times, complicate the identification of different neuron types. Robust classification schemes are likely to circumvent this problem, by allowing same cell-types to be studied repeatedly [2]. In model organisms, such classification will enable genetic access, allowing neurons to be marked and manipulated, especially in species in which transgenesis is advanced, such as flies, worms, mice and zebrafish. Molecular profiling and the development of tools for specific cell-types' access are invaluable for understanding development, – to overcome the difficulty in unraveling the steps in which a neuron takes up its final form and function, evolution, – among model organisms and humans, and disease – by the identification of cell-types most vulnerable in neurological disorders [3].

Intuitively, neurons could be grouped into a type, were they to serve a particular function that is different from another type of neurons. However, since some functions seemingly emerge at circuit levels, a more global definition of a neuronal type is a population of neurons that exhibit properties that are homogenous within that type, but different from another. Relevant properties that help define a population as a type also include the morphology – dendritic structure, soma size and axonal projections, physiological properties – resting potential and

firing rate, molecular properties – protein and mRNA composition, and a fourth parameter of connectivity which is relatively harder to assess [3].

1.2 The visual system in zebrafish

One of the neuronal circuits that has had scientists engaged in decoding for decades now is that of the visual system. The zebrafish retina is used as a model to study visual systems, since the retina provides a neuronal circuit that is isolated from the rest of the nervous system, allowing the conversion of information from a controllable sensory input to a single output [4]. The zebrafish (*Danio rerio*) is an important model for neuroscience for several reasons. Zebrafish are prolific breeders, with a rapid rate of development. Additionally, since their eggs are transparent, embryos can be studied without disrupting development. Important questions of development and genetics in complex organisms such as vertebrates can be easily explored by using zebrafish, which additionally offer a high degree of genetic tractability [5].

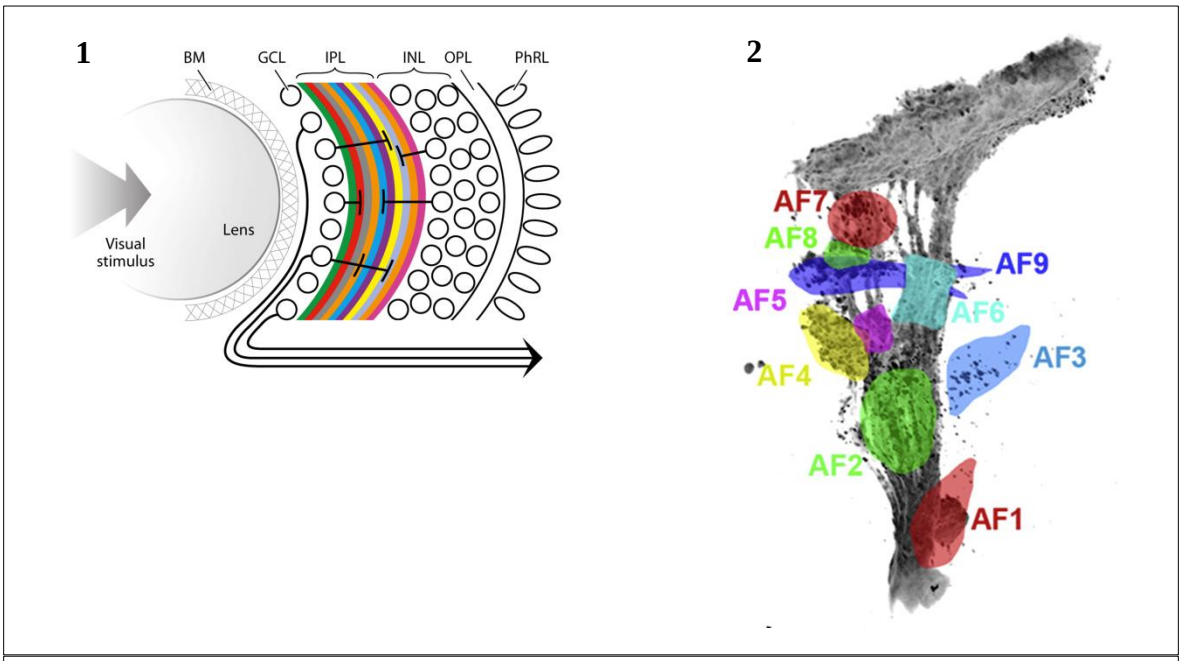

Figure 1: The zebrafish visual system. 1) The anatomy of the eye, illustrating the laminar organization of the retina. 2) The 10 retinorecipient regions or arborization fields of the visual system, labeled AF 1-9, with AF 10 being the most dorsal arborization field, i.e., the optic tectum (modified from Baier, 2013 and Robles et al., 2014)

The zebrafish retina also appears to be similar to other vertebrates. A particularly important feature of the retina is that most retinal neurons are arranged in a mosaic pattern [6]. This mosaic spacing of neurons wherein neurons of a single type are randomly spaced relative to neurons of another type offers a criterion for grouping neurons into types, independent of other conventional parameters of physiology or molecular properties.

The retina consists of three nuclear layers and two plexiform layers, as shown in Figure 1.1. The outer nuclear layer (ONL) comprises the photoreceptor cell bodies, while the inner nuclear layer (INL) contains the cell bodies of the amacrine, bipolar and horizontal cells. The ganglion cell layer (GCL) consists of the retinal ganglion cells (RGCs), which are the output neurons of the visual system. Synaptic connections arise between these nuclear layers, in the plexiform layers. The outer plexiform layer (OPL) connects the photoreceptors with the bipolar and horizontal cells while the inner plexiform layer (IPL) consists of synaptic connections between the amacrine, bipolar cells and the RGCs [7].

1.3 Retinal ganglion cells as the output neurons of the visual system

RGCs are the output neurons of the visual system. Each ganglion cell is considered to host the output of specific visual processing step by the retina. Thus, characterizing each type of RGC would provide a complete schematic of what the eye tells the brain [8]. This will not only further our understanding of the visual system, but also improve our understanding of what constitutes a type [9].

RGCs share several features, with their cell bodies situated in the ganglion cell layer and their dendrites arborizing in the IPL, and axons traversing to the contralateral optic tectum in the brain. RGCs innervate ten different retinorecipient areas in the tectum (Figure 1.2) and a single RGC is able to innervate multiple, different visual areas in the brain through its axon collaterals [10]. This is intriguing because it means that different RGCs are specialized for different visual features, and are able to transmit highly processed information, in parallel, to the retinorecipient regions of the brain [11]. RGCs also display heterogeneity in terms of their responses to fluctuations in light intensity, orientation and direction of stimuli [8,11–14]. Over many decades, several landmark findings have come to contribute to the understanding of the structure-function relationship between neurons, with the finding that

RGC arborization layers link structure to function and that different physiological types are linked to specific morphological types [15].

Neuronal classification of RGCs relies on four parameters. The primary one is of course, morphology [16]. Morphological classification, in turn, includes parameters such as, length and width of the cell body, the depth and thickness of stratification, the total width of the stratification and the dendritic branching pattern. These classification criteria generated a catalogue of eleven well defined RGC types [17]. Another criterion being increasingly used today is the molecular signatures of the RGCs, although it is still uncertain as to whether a single gene might be able to mark a single type [18]. Physiology and connectivity are the other two parameters which definitely present their own challenges in their utilization as mapping parameters [3].

1.4 The retinal projectome

Pioneering work has been able to successfully generate the first cellular resolution connectivity map between the retina and the brain [19]. The retinal projectome maps the RGCs in terms of their dendritic morphology and their axonal projection classes, to provide a wiring diagram of the organizing principles of the visual system in zebrafish [20]. The retinal projectome defined twenty stereotyped projection patterns, of which a majority innervated multiple visual areas of the brain. More than fifty RGC types were identified that had unique combinations of dendritic morphology and axonal projection classes, indicating that certain projection patterns are non-homogenously specified in the retina to generate biased visual maps in the brain [12,21,22]. Thus, these single-cell projection mapping data, as shown in Figure 2, provide a catalogue of brain-area-specific visual representatives and a blueprint for physiological characterization and analyses of specific RGC types.

While the morphological atlas allows us to partly elucidate the visual circuitry, monitoring and manipulating individual RGCs within larger, defined populations requires precise genetic access [23]. One of the methods becoming increasingly popular for the same is high-throughput molecular profiling [24].

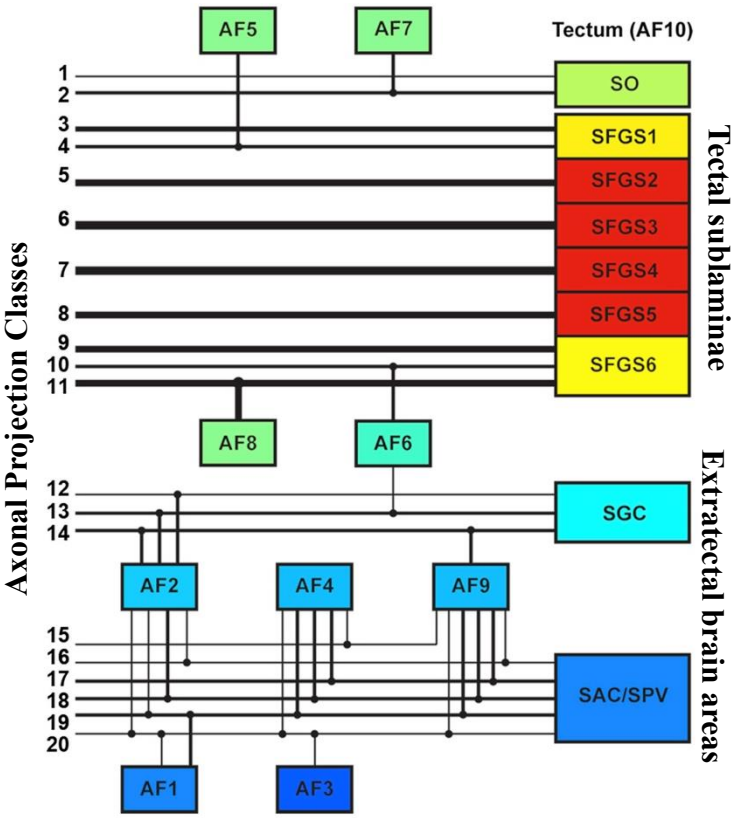

Figure 2: **Wiring diagram of RGC projections in the larval zebrafish brain**
This wiring diagram shows how RGC types may innervate multiple regions within the optic tectum, and the extratectal brain regions in defined projection patterns, and also arborize into 9 other arborization fields marked AFs 1-9 (modified from Robles et al., 2014).

1.5 High-throughput single-cell RNA-sequencing

Several advances in single-cell genome-wide molecular profiling techniques have boosted the efforts directed at cell-type classification [24]. These techniques profile the genome, transcriptome and epigenome of single cells with a great degree of sensitivity. Molecular profiling often reveals the diversity that may be masked by averaging across large cell populations, along with an unbiased coverage. The most robust of these techniques, which is easily scalable is single-cell RNA-sequencing (scRNA-seq) [25].

To perfrom scRNA-seq, cell dissociation and sorting is performed using microfluidics and fluorescence-activated cell sorting (FACS). Subsequently RNA is converted to cDNA which is further amplified and sequenced. This method has been successfully used for the

comprehensive classification of bipolar cells in mouse retina [26], and has been recently utilized for generating the molecular profile of zebrafish RGCs as well. The retina is first homogenized and cell-dissociation is performed. The cell suspension is enriched for RGC populations by FACS, and then introduced into a microfluidic device. Within this device, an oligonucleotide labeled or 'barcoded' bead and a single RGC are encapsulated in a nanoliter droplet, so that the beads collect and barcode the RGC mRNA [27]. Upon lysis, large scale reverse transcription occurs, followed by cDNA amplification and subsequent sequencing for thousands of RGCs. This generates a molecular profile to which principle component analysis can be applied to generate a t-SNE plot as shown in Figure 3.

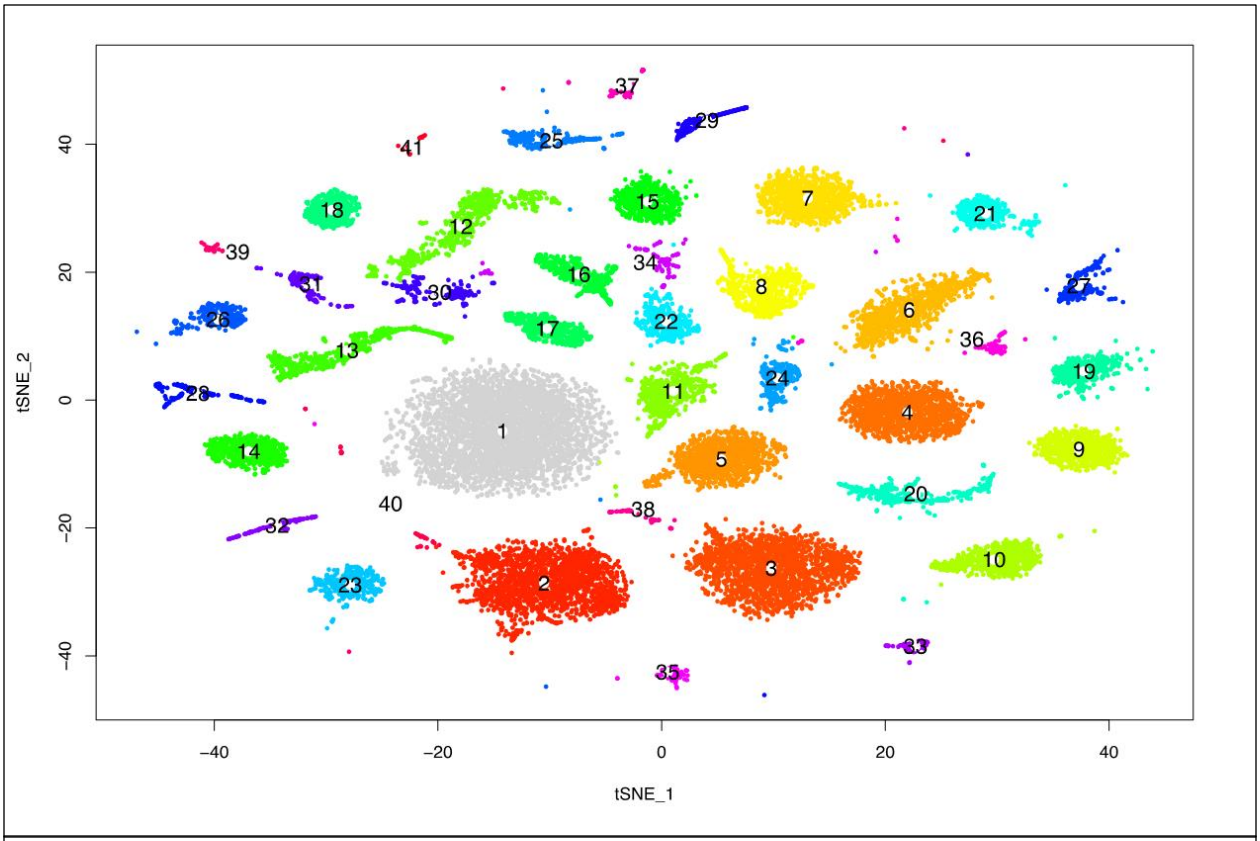

Figure 3: **Molecular profiling reveals 41 putative molecular markers for RGC types.** PCA applied to the scRNA-seq data reveals 41 clusters of cells, clustered by the similarity of their transcriptional domains. Each dot within a cluster represents a cell, and thus a cluster of cells indicates the similarity in their mRNA transcripts.
(Collaboration Baier and Sanes, unpublished)

Analysis of the data generated from the scRNA-seq of ~22,600 RGCs revealed 41 putative markers for RGC types, which could be further surmised in the dot plot shown in Figure 4. The dot plot shows the putative makers, which could serve as genetic access points to the genes in rows and the clusters that they appear in, in columns. The size of the dot represents the percentage of cells within the cluster that express the gene, with the color of the dot representing the percentage of transcripts of the same gene, normalized to 1. Some of the genes were more specifically expressed within one cluster than the other, and such genes with clean genetic signatures could potentially be used and validated as tools for genetically accessing morphologically classified RGC types in zebrafish retinas.

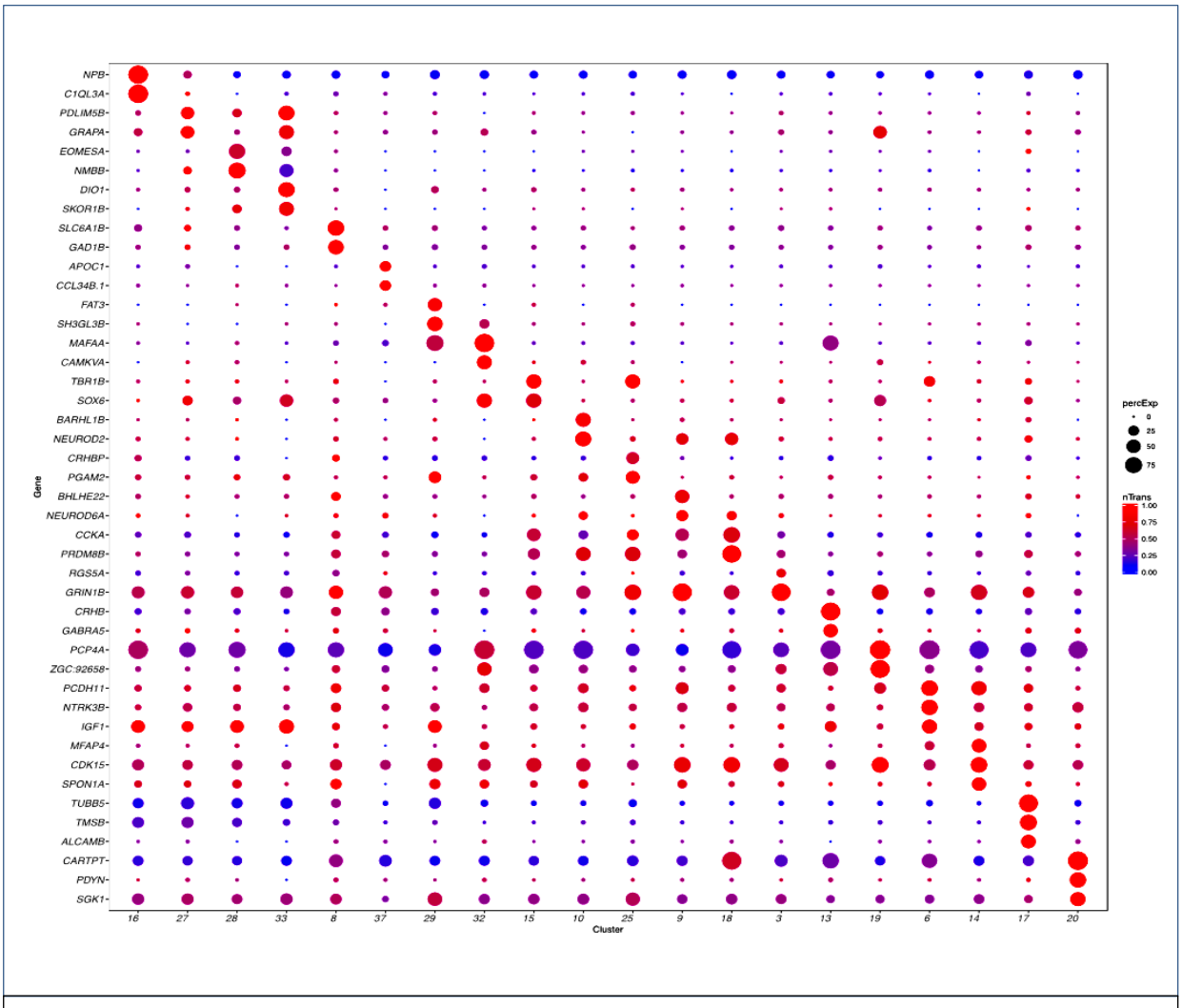

Figure 4: **Differentially expressed genes as potential markers of RGC types.** The dot blot shows genes in rows against the clusters in which they are expressed in columns. (Collaboration Baier and Sanes, unpublished)

The high-throughput scRNA-sequencing data thus caters to the second parameter of neuronal cell-type classification, i.e., the molecular signatures. However, classification requires the establishment of correspondence between morphology and molecular profiles [1], and thereby the validation of the genes that have been generated through scRNA-seq as markers of RGC types. This will then pave the way for establishing correspondence between more complex and variable properties such as physiology, function and connectivity.

Such correspondence can be established using the wide array of transgenic tools that are at the disposal of scientists, such as *in situ* hybridization [28] coupled with sparse labeling techniques and genome editing techniques such as CRISPR/Cas9 [29]. This review will focus on the use of a homology independent targeted integration-mediated CRISPR/Cas9 transgenesis [30] that has been used for the validation of the candidate genetic markers of RGC types in zebrafish.

1.6 Homology independent targeted integration-mediated CRISPR/Cas9 transgenesis

Site-specific integration of a transgene can be achieved using the homology dependent pathway of cell repair which relies on the presence of short homologous fragments [31]. However, this method is inefficient and more importantly, cannot be used for non-dividing cells. In contrast to this, a homology-independent approach offers by non-homologous end joining, a way to repair double-stranded breaks in both proliferating and post-mitotic cells. It is also more efficient than the homology-directed repair [30]. Genetic knock-ins can be carried out exploiting the intrinsic precision of the non-homologous end joining repair, as has been used for the validation of genetic markers for RGC types. This method has been designated herewith as homology independent targeted integration or HITI.

As shown in Figure 5, the HITI-mediated CRISPR/Cas9 approach is used to express GFP from the endogenous marker loci. Thus, the HITI donor plasmid along with the Cas9/gRNA complex is co-injected into the single-cell stage of a zebrafish reporter line incross. The driver and reporter lines used are of the Q system [32], wherein QF2 is the driver, which drives its upstream activator sequence – QUAS, to regulate expression of the genes adjacent to it. The genome editing occurs such that two concurrent cuts are made – one in the genome and the other in the HITI donor plasmid. What is intriguing about the construction of the

HITI donor plasmids is that it circumvents error-prone integrations of the transgene by allowing successful integration only in the forward orientation and not the reverse, since an intact gRNA target sequence remains in the latter and is cleaved by the Cas9 endonuclease, until forward transgene integration occurs, or indels occur that prevent further gRNA binding [30].

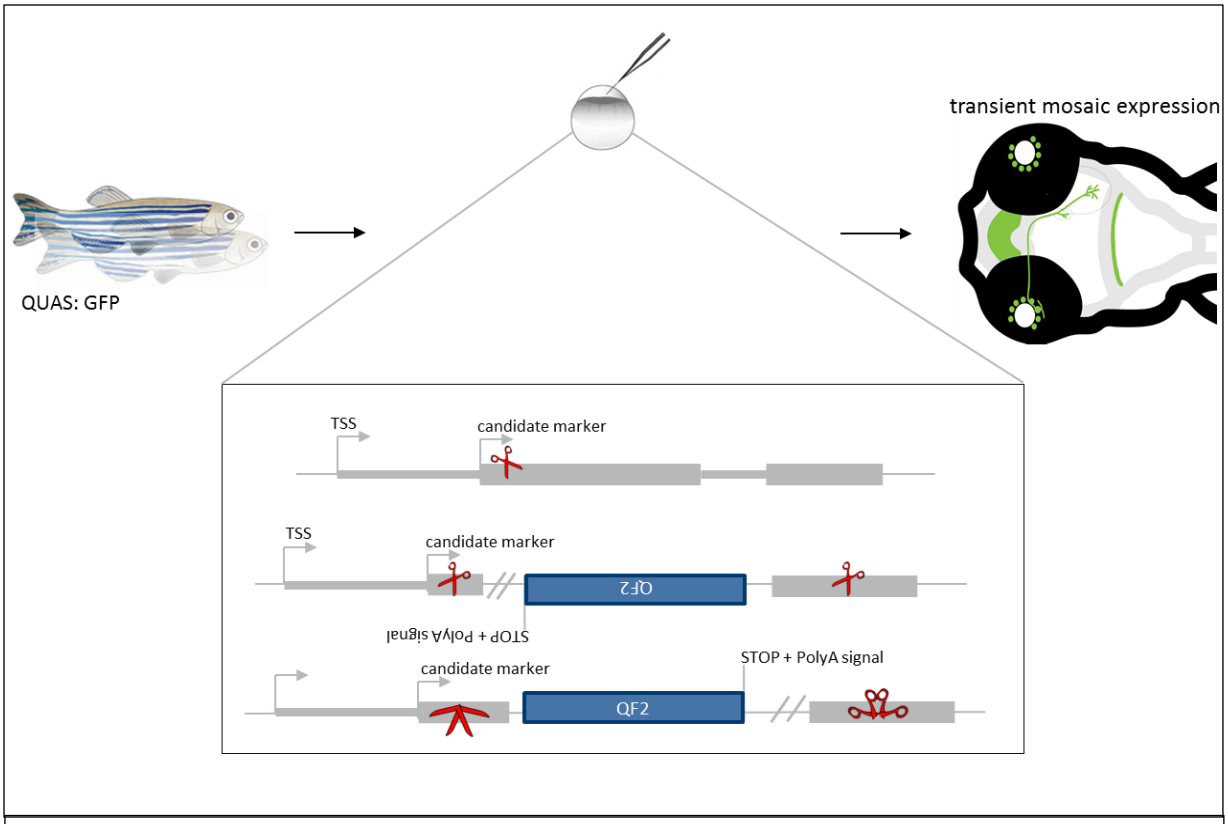

Figure 5: **HITI-mediated CRISPR/Cas9 approach.** The schematic illustrates the workflow of using transgenesis to express GFP from the endogenous maker loci. Only when the transgene is integrated in the forward orientation, does a successful knock-in occur, enabling the visualization of transient GFP expression in zebrafish larvae.

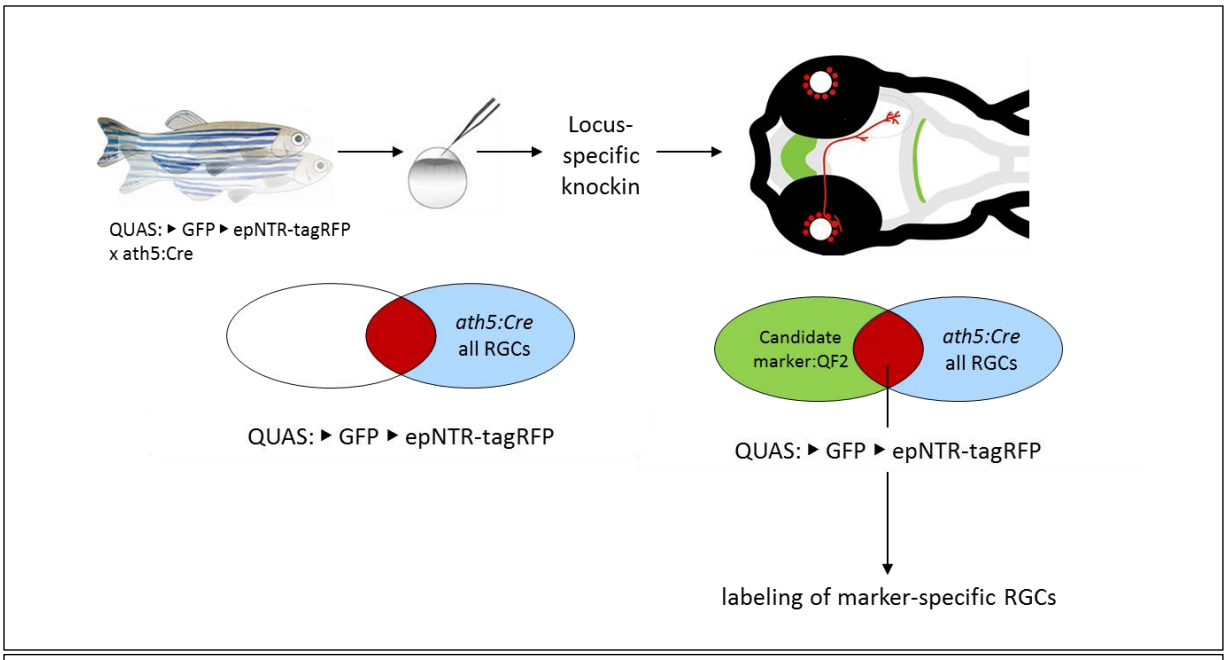

Figure 6: **An intersectional approach allows labeling of marker-specific RGC types.** The reporter line is crossed with a Cre line, that mediates recombination in RGCs, such that all cells expressing the marker are GFP-labeled, whereas only the RGCs expressing the marker are RFP-labeled.

Of course, this technique enables the labeling of all cells that may express the marker gene, and therefore restriction of expression requires an intersectional genetic approach [33,34] as has been used in this study (Figure 6). This approach makes use of two binary systems. One is the aforementioned Q system and the other is the Cre/lox system [35]. A reporter line carrying a GFP cassette flanked by two *loxP* sites is crossed with a *Cre* line that mediates recombination in RGCs alone. Thus, RGCs are labeled where the Q system and the Cre/lox systems' expression patterns overlap. Since, the reporter gene also carries an RFP label on the same construct, marker-specific RGCs acquire RFP-labeling within a population of GFP-labeled cells expressing the marker gene.

Such expression patterns will enable the visualization of type-specific RGCs, and enable the study of their roles in visual pathways with the use of ablation and functional imaging tools such as the enhanced potency nitroreductase (*epNTR*) encoded within the novel transgenic lines [36–38]. The present study focuses on the establishment of transgenesis for mapping the potential candidate markers onto morphologically classified RGC types.

CHAPTER 2: GENESIS OF HYPOTHESIS AND OBJECTIVES

Genesis of hypothesis:

Retinal ganglion cells (RGCs) were comprehensively classified based on their dendritic morphology and axonal projections. This presented an intriguing finding that, both dendritic stratification and axonal projection patterns contribute to the parallel processing of visual information. To characterize these functionally and morphologically distinct neurons, it is crucial to have access to them, which is where molecular profiling proves to be adept. High-throughput single-cell RNA-sequencing data of adult zebrafish RGCs has revealed differentially expressed genes that could serve as genetic entry points to access and manipulate different RGC types. Thus, the present study focuses on the establishment of methods to map the molecular markers of RGC types onto their morphologically classified types.

Objectives:

To establish techniques to map genetic markers of RGC types onto their morphologically defined classes, using *in situ* hybridizations and locus-specific homology independent targeted integration-mediated CRISPR/Cas9 transgenesis, to express GFP from the endogenous markers' loci. To then study the morphology of marker specific RGC-types, using intersectional genetic approaches and thus generate novel transgenic lines that will enable the functional analyses of RGC types.

CHAPTER 3: MATERIALS AND METHODS

3.1 Equipment and consumables

The general laboratory equipment and the consumables used in this work are listed:

General equipment: Analytik Jena PCR Thermal Cycler

Eppendorf tubes: 1.5ml, 2ml

Falcon tubes: 10ml, 50ml

Greiner Bio-One, 6-well plates

Hettich MIKRO 120 Microlitre Centrifuge SMART RUNNER

Hettich MIKRO 220 & 220R Microliter Centrifuge

Kisker Biotech GmbH & Co. KG Thermoshaker TS 100C

Kisker Biotech GmbH & Co. KG Vortex V1 Plus

Mettler Toledo Pipet-Lite XLS + Multichannel pipettes

Rainin, Pipettes (1000µl, 200µl, 20µl, 10µl)

Roth, Pasteur Pipette

SPROUT Mini Centrifuge 12V

Thermo Scientific, Heraeus Incubator

SemperGuard, Latex Gloves

SemperGuard, Nitrile Gloves

Microinjection: Eppendorf, Microloader pipette tips

Harvard Apparatus GC 100F-10, Glass Capillaries

World Precision Instruments, Pneumatic Picopump PV820

Stutter Instruments, P-97 Needle Puller

Microscopy: Carl Zeiss LSM-780 confocal microscope

Leica, MDG 36 (stereomicroscope)

	Zeiss, Stemi 2000 (stereomicroscope)
Software:	ImageJ FIJI
	Graph Pad, Prism
Zebrafish	Techniplast, Zebrafish Research Systems
husbandry:	Greiner Bio-One, Petri Dish 96mm

3.2 General Reagents and Enzymes

Agarose (Biozyme), Ampicillin, Glycerol, Maleic acid (Roth), Dimethylsulfoxide, Ethyl alcohol, Methyl alcohol, Formamide, Triton X-100, Tween-20 (Sigma Aldrich), Metrodinazole (Fluka), Yeast extract, Hydrochloric acid (Merck), NBT/BCIP, Anti-DIG-AP (Sigma Aldrich), Proteinase K (Genaxxon), RNasin (Promega), Trypsin, NotI-HF, Sp6 RNA-Polymerase (New England Biolabs), CRISPR/Cas9 tracrRNA, CRISPR/Cas9 crRNA, Cas9 nuclease (IDT)

3.3 Solutions and Buffers

The composition of solutions and buffers are listed in the following:

Blocking Buffer: 1x Blocking Reagent, 2mg/ml BSA, 2% sheep serum, 0.1% DMSO in PBST

Blocking Buffer Stock [10X]: Blocking Reagent (Roche) 10% in Maleic acid buffer.
Heat to dissolve. Do not boil.

E3 Embryo medium: 5mM NaCl, 0.17mM KCl, 0.33mM CaCl2, 0.33mM MgSO4. Add 2 drops Methylene blue per eight-liter tank

Hybridization mix: 50% formamide, 5x SSC, 5 mg/ml Torula RNA, 50 µg/ml Heparin, 0.1% Tween 20 in 250ml H_2O. pH 6-7

LB (Agar): 5g/L Yeast extract, 10g/L Trypton, 0.5g/L Sodium chloride, 15g/L Agar. pH 7.0

Maleic acid buffer: 100mM Maleic acid, 250mM NaCl. Adjust pH to 7.5 with NaOH

MESAB: 4% Tricaine (ethyl 3-aminobenzoate) in distlilled H2O. pH 7.0 (Tris-HCl buffered)

PBS: 140mM Sodium chloride, 2.7mM Kalium chloride, 10mM Disodium phosphate, 1.8mM Monopotassium phosphate. pH 7.2

PBST (PBS – Triton (0.25%)): PBS 1L + 2,5ml Triton

4% PFA in PBS: Dilute 16% PFA vial 1:4 in PBS

Proteinase K solution: Dilute ProteinaseK [20mg/ml] 1:2000 in PBST

20X SSC: 3M NaCl, 300mM NaCitrate in 1L Millipore Milli-Q water.Adjust pH 7.0 with HCl

Staining Buffer: 1ml 5M NaCl, 5ml 1M $MgCl_2$, 2.5ml 1M Tris-HCl, pH 9.5, 50µl Tween-20, in 50ml H_2O

TAE-Buffer: 40mM Tris, 20mM Acetic acid, 1mM EDTA. pH 8.0

TNT: 100mM Tris, 150mM NaCl, 0.5% Tween-20 in 1litre H_2O. Adjust pH with HCl to 7.5

TNTB: 1% Blocking Reagent in TNT

3.4 Oligonucleotide sequences and applications

Primers for the synthesis of a RNA sense probe were used for *in situ* hybridizations, and were provided by Eurofins, with sequences as shown in Table 1 for 8 candidate marker genes – *barhl1b*, *bhlhe22*, *c1ql3a*, *cart3*, *eomesa*, *mafaa*, *pdyn* and *tbr1b*. Table 1 also has the gRNA target sites for the oca2 knock-out, and the *barhl1b* and *eomesa* knock-ins.

Name	Gene name	Sequence (5'→3')	Application
barhl1b_fwd	BarH-like homeobox 1b	ATTTAGGTGACACTATAG ATGGAAGCGTCCACCAAC	RNA probe
barhl1b_rev		TAATACGACTCACTATAGGG TCTGAATTGTGCCGTTCATC	RNA probe
bhlhe22_fwd	basic helix-loop-helix family, member e22	ATTTAGGTGACACTATAG CTGCGGGTATTGATCTTTCC	RNA probe
bhlhe22_rev		TAATACGACTCACTATAGGG TGGTTGCATGTTGTCAGGTC	RNA probe

c1ql3a_fwd	complement component 1, q subcomponent-like 3a	ATTTAGGTGACACTATAG GTGCTGGTCATCCTCATCC	RNA probe
c1ql3a_rev		TAATACGACTCACTATAGGG TTGCTTCCTTTCCAGCTTTC	RNA probe
cart3_fwd	cocaine- and amphetamine-regulated transcript 3	ATTTAGGTGACACTATAG ATGACCATGGAGAGTTCCAAAATC TG	RNA probe
cart3_rev		TAATACGACTCACTATAGGG TGCTCGAGAAAACACAGAAAC	RNA probe
eomesa_fwd	eomesodermin homolog a	ATTTAGGTGACACTATAG TTCGTCGTCTCTGCATTACG	RNA probe
eomesa_rev		TAATACGACTCACTATAGGG CGAATCTTCGCTCTGAGGAG	RNA probe
mafaa_fwd	v-maf avian musculoaponeurotic fibrosarcoma oncogene homolog Aa	ATTTAGGTGACACTATAG CACCGATCTCGCCATGAG	RNA probe
mafaa_rev		TAATACGACTCACTATAGGG TACGTTGGTGAGGGGAAAAG	RNA probe
pdyn_fwd	prodynorphin	ATTTAGGTGACACTATAG ATTTGGACTCTGCGGTGAAC	RNA probe
pdyn_rev		TAATACGACTCACTATAGGG CATATGGGGAAAAGTCAACG	RNA probe
tbr1b_fwd	T-box, brain, 1b	ATTTAGGTGACACTATAG GAGCAACTCTTCTCCGCAAG	RNA probe
tbr1b_rev		TAATACGACTCACTATAGGG	RNA probe

		AAAGTCCAGTCGGTTGTTGG	
oca2_T1	Oculocutaneous albinism II	GTACAGCGACTGGTTAGTCATGG	gRNA target site
barhl1b_T1		TCCAAAACTGGAGCCGTTGGTGG	gRNA target site
eomesa_T5		GGACAGGTTGTAGAAGGTCTTGG	gRNA target site

3.5 Zebrafish lines

Casper WT larvae were used for colorimetric *in situ* hybridizations, *oca2* knock-outs and Nacre (*mitfa*$^{-/-}$) for all outcrosses. The transgenic lines *Tg(QUAS:GFP$_{CAAX}$)* and *Tg(ath5:Cre)* were used for the HITI-mediated CRISPR/Cas9 transgenesis. *Tg(QUAS:loxP-GFP-loxP-epNTR-tagRFP),* hereby labeled *Tg(QUAS: ▸ GFP ▸ epNTR-tagRFP)* was used for intersectional genetic approaches. All experiments were conducted with 5dpf larvae. Since gonadal discrimination has not occurred at this stage, males and females were used indiscriminately.

3.6 Zebrafish maintenance, mating and breeding

The zebrafish were maintained in a recirculating aquaria system. The water temperature was maintained at 28.5°C. The water was sterilized through a UV lamp, and filtered to remove any excrement. Environmental conditions of pH, salt concentration and nitrogen derivative concentration were tested regularly. The illumination was adjusted to a 14h-light and 10h-dark cycle. The zebrafish were fed with *Artemina salina*, and dry food three to four times a day. The tanks were cleaned as necessary.

Zebrafish mating was done over two days. The male and female zebrafish were placed in a mating box overnight, separated by a divider. The divider would be removed the following day, to enable mating, which was generally induced by light stimulation. A sieve was used to prevent the spawning of eggs. The zygotes were collected in 9cm Petri plates, with a zygote density of 60/plate.

The embryos to be raised were raised in Danieau's solution (17 mM NaCl, 2 mM KCl, 0.12 mM $MgSO_4$, 1.8 mM $Ca(NO_3)_2$, 1.5 mM HEPES) at 28.5°C on a 14/10 light/dark cycle. Those to be used for transgenesis and hybridization experiments were raised in PTU (phenylthiourea) to suppress pigmentation and keep the larvae transparent.

All animal procedures conformed to the institutional guidelines of the Max Planck Society and the local government (Regierung von Oberbayern).

3.7 RNA probe synthesis and purification

RNA probe templates were prepared using Phusion PCR, and cloned into a pcrII-vector with the Dual Promoter TA Cloning Kit from Invitrogen. The TOPO cloning product was transformed into competent *E.coli* cells. The presence of the insert was determined by blue-white screening using X-Gal as a substrate. Single white colonies were picked from the agar plate using sterile pipette tips and cultured overnight. The plasmids were purified, Not-1 HF restriction digested and sequenced with M13 reverse sequencing. The sequences that aligned in reverse orientation were chosen for all candidate marker genes. The DIG-RNA labeling mix was used, wherein 1µg linearized plasmid was mixed with 2µl transcription buffer [10x], 2µl DIG-RNA Labeling Mix [10mM ATP, 10mM GTP, 10mM CTP, 6.5mM UTP and 3.5mM DIG-UTP], 2µl Sp6 RNA-polymerase [20U/µl], 1µl RNasin and nuclease-free distilled water to final volume of 20µl. Transcription took place at 37°C for one hour. The DNA-plasmid was digested by adding 2µl DNaseI and further incubation at 37°C for one hour. The RNA probe was purified using the Machery Nagel RNA Clean-up kit and the quality was checked by gel electrophoresis. 20µl formamide were added to the probe to prevent degradation. The DIG-labeled sense RNA probe was diluted 1:500 in Hybridization mix for the colorimetric *in situ* hybridizations.

3.8 Preparation of 5dpf larvae for whole mount colorimetric *in situ* hybridizations

Casper WT larvae were anesthetized in MESAB and fixed in 4% PFA overnight, at 4℃. 3x5minute washes in PBST were performed, and this was followed by sequential dehydration and rehydration series with Methanol. The larvae were then bleached with 3% H_2O_2 in PBST for 30 minutes on a shaker, at RT. The larvae were permeabilized using Trypsin-PBST (1:20 dilution) for 45 minutes on ice, washed and then post-fixed in PFA-PBST. The larvae were washed once again after post-fixation and then pre-hybridized for 2-5 hours in the Hybridization mix at 65℃. The larvae were then hybridized in the hybridization mix containing the DIG-labeled probes overnight, at 65℃. This was followed by a series of stringency washes to remove any unbound or wrongly-bound probes, after which the larvae were blocked in the blocking buffer for 2-3 hours. The larvae were then incubated overnight with anti-DIG-AP (1:5000) in blocking buffer, at 4℃. After a series of PBST washes, the larvae were equilibrated using Tris-Cl, followed by a quick incubation in the staining buffer. The larvae were then incubated in NBT/BCIP in staining buffer, at RT until staining occurred. They were then given PBST and methanol washes, and then post-fixed in PFA before being cleared and stored in glycerol. The larvae were imaged at the Leica, MDG 36 (stereomicroscope).

3.9 *In vitro* test of gRNAs

To ensure that the gRNAs designed using CCTop [39] (https://crispr.cos.uni-heidelberg.de/) were on-target, the *barhl1b, eomesa, c1ql3a* and *pdyn* plasmids were restriction digested with Not1-HF, and NEB Cas9 protein was then used to digest the plasmid DNA, using the gRNAs designed. This enabled us to check whether Cas9 could recognize the on-target gRNA site and cleave the plasmid DNA. For performing the *in vitro* test, the gRNA and Cas9 protein were incubated for 10 minutes, at 25℃, to allow gRNA to complex with the Cas9 nuclease. The substrate DNA was then added to the reaction mix, and it was incubated at 37℃ for 15-30 minutes. The reaction was stopped by adding ProteinaseK, and the plasmid DNA was run on a 1% agarose gel.

3.10 Checking the efficiency of CRISPR/Cas9 reagents

The knock-out efficiency of Cas9 protein and Cas9 mRNA was tested by knocking-out *oca2*, a gene encoding for melanosomes. To test the efficiency of Cas9 protein for an *oca2* knock-out, the tracrRNA and crRNA were annealed in a 1:1 ratio in a Duplex buffer, at 95℃. The gRNA formed was then complexed with Cas9 protein in a 1:1 ratio by 10 minute incubation at 37℃. To check the efficiency of the Cas9 mRNA, it was added to the freshly prepared gRNA to prepare the injection solution. Each of the CRISPR/Cas9 injection solutions were injected into single-cell stage embryos of WT larvae as described in 3.12.

3.11 Cloning of donor plasmid for QF2 knock-in to *barhl1b* and *eomesa* loci

The Golden GATEway cloning protocol [40] was followed for all knock-ins that were performed in this study, including the test of knock-in efficiencies.

Golden GATEway Cloning Vectors:

EV1: GFP gRNA

EV2: gRNA sequence (as annealed oligos)

EV3: Linker

EV4: QF2 donor plasmid

EV5: PolyA tail

Golden GATEway Assembly: 50ng of each of the vectors were sequentially assembled, in a reaction mix containing 1µl each of the FD (10X) Buffer and T4 (10x) Ligase Buffer, and 0.6µl each of the BsaI FD and T4 Ligase in a final volume of 20µl.

To check the knock-in efficiency of the Cas9 protein, crRNA and tracrRNA were annealed in a 1:1 ratio, at 95℃. The Cas9 protein was diluted in its working buffer, and incubated with equal volumes of the gRNA, at 37℃, for 15 minutes. The QF2 donor plasmid, prepared by Golden GATEway cloning was added at a concentration of 20ng/µl. This cocktail was then injected into single-cell stage embryos harvested from a QUAS:GFP incross.

To check the knock-in efficiency of Cas9 mRNA, crRNA and tracrRNA were annealed in a 1:1 ratio, at 95℃. The Cas9 mRNA was added to the freshly prepared gRNA. The QF2 donor plasmid, prepared by Golden GATEway cloning was added at a concentration of 20ng/µl. This cocktail was then injected into single-cell stage embryos harvested from a QUAS:GFP incross.

3.12 Microinjections

Microinjections were performed to co-inject the Cas9/gRNA complex along with the HITI-donor plasmid into developing embryos. Microinjections were performed on freshly laid eggs up to the two-cell stage. The eggs were sorted on a 1.5% agarose-Danieau's solution mold. Following injections, the eggs were incubated at 28℃, and sorted for fertilized eggs after 3-4 hours when the embryos were further along in development.

3.13 Image acquisition and analysis

For live imaging, 5dpf larvae were embedded in 1% low-melting agarose and imaged using a Carl Zeiss LSM-780 confocal microscope, equipped with lasers for excitation of EGFP (488nm) and mCherry (543nm). Image analysis was performed using ImageJ FIJI software.

3.14 Visual Background adaptation assay

5dpf larvae from a *ath5:QF2, QUAS:epNTR, ath5:Cre* outcross were sorted for RFP + (test) and RFP – larvae (control). Both were incubated in Metronidazole (MTZ) for 48 hours at 28.5℃, in the dark. Both the test and control groups were then imaged at the Carl Zeiss LSM 780, to check for RGC ablations, and then presented with a white background to test their visual adaptation.

CHAPTER 4: RESULTS

4.1 Characterization of endogenous expression patterns of marker genes

Endogenous expression patterns of the 8 candidate marker genes characterized with whole mount colorimetric *in situ* hybridization performed on 5dpf PTU treated and bleached *Casper* WT larvae have been shown in Table 2. This table also describes the candidate marker genes' functions and expression domains. The characterization of the endogenous expression patterns of marker genes provided a framework for more confident transgenesis.

4.2 Establishment of the HITI-mediated CRISPR/Cas9 approach

4.2.1 *In vitro* test of gRNAs

As seen in Figure 7.1, the gRNAs synthesized using CCTop were on-target, were cleaved by Cas9. Other than the control, all tested gRNAs show three bands, corresponding to the restricted plasmids themselves and the two Cas9 cleaved fragments.

4.2.2 Knock-out efficiency of Cas9 protein versus Cas9 mRNA

As seen in Figure 7.2, the larvae injected with the Cas9 protein/gRNA complex showed a loss of melanosomes encoded by *oca2*, as opposed to those injected with Cas9 mRNA/gRNA complex which resembled the WT. Thus, using a Cas9 protein/gRNA complex was more efficient in generating knock-outs (Figure 7.3), as opposed to Cas9 mRNA which in fact was more lethal and absolutely inefficient.

4.2.3 Knock-in efficiency of Cas9 protein versus Cas9 mRNA

Knock-ins with both candidate marker genes under investigation were performed using Cas9 protein/gRNA complex and Cas9 mRNA/gRNA complex. The rationale behind this test was to determine whether Cas9 mRNA/gRNA complex would be more efficient, since it would bind to the target site and start cleaving the donor plasmid only after the CRISPR/Cas9 cocktail along with the HITI donor plasmid had been injected into the single-cell stage embryo, enabling a more delayed strategy of transgenesis, and a more mosaic expression pattern of the transgene. This would, in theory, be more favorable than the Cas9 protein/gRNA complex which could start cleaving the HITI donor plasmid at once.

However, we found that the Cas9 protein/gRNA complex was more efficient in generating successful knock-ins as opposed to Cas9 mRNA for both *barhl1b* and *eomesa* (Figure 7.4).

Gene name	Gene function	Gene expression pattern	Gene expression domains
barhl1b	Regulation of transcription by RNA Pol II	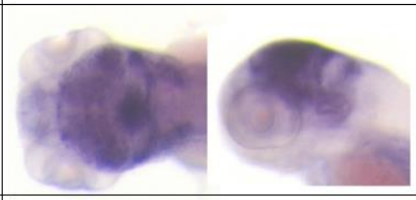	Forebrain, midbrain, optic tectum, GCL
bhlhe22	Regulation of transcription by RNA Pol II	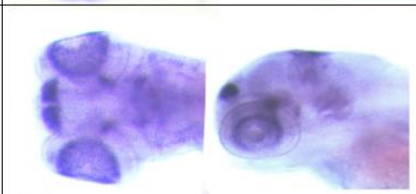	Forebrain, midbrain, hindbrain, optic tectum, GCL
c1ql3a		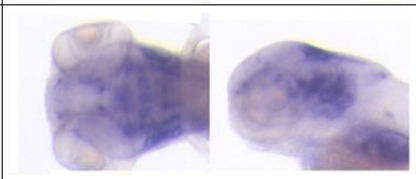	
cart3	Neuropeptide hormone activity	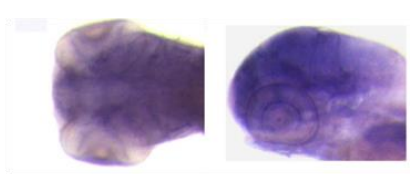	Forebrain, midbrain, hindbrain, lens, GCL
eomesa	DNA binding	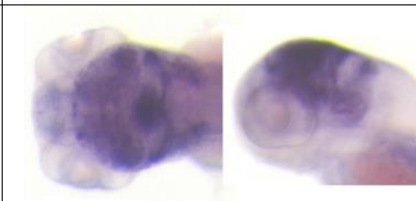	Forebrain, midbrain, hindbrain, optic tectum, GCL
mafaa	Sequence-specific DNA binding	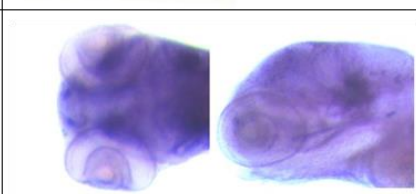	Forebrain, midbrain, hindbrain, optic tectum, GCL
pdyn	Opiod receptor binding	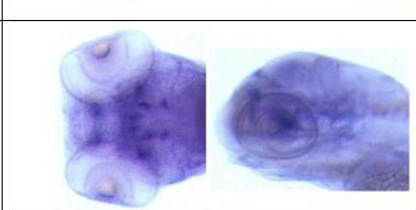	Forebrain, midbrain, GCL
tbr1b	DNA binding	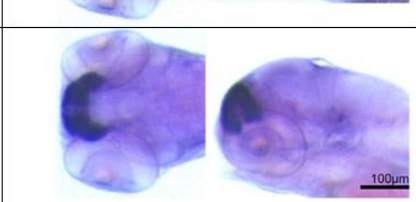	Forebrain, GCL

Table 2: Characterization of endogenous expression patterns of marker genes

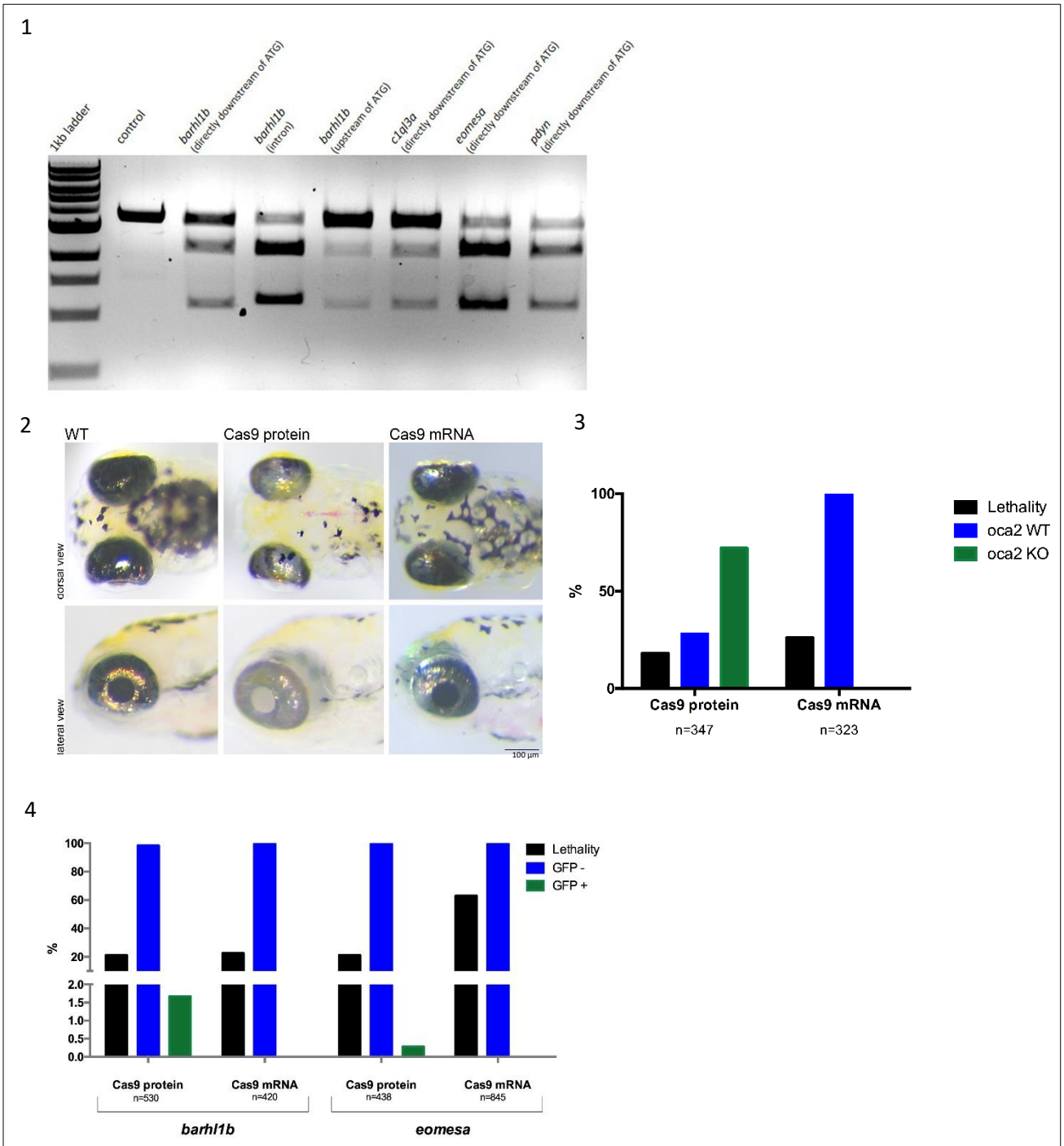

Figure 7: Establishment of the HITI-mediated CRISPR/Cas9 approach. 1) gRNAs synthesized using CCTop were tested and found to be recognized and cleaved by Cas9. 2-4) Cas9 protein/gRNA complex was more efficient for knock-outs of *oca2* and knock-ins at the endogenous loci of the candidate marker genes – *barhl1b* and *eomesa*

4.3 Characterization of transient gene expression reflects endogenous gene expression patterns

Successful integration of the Cas9 protein/gRNA complex and the HITI donor plasmid containing QF2, was able to drive GFP expression from the endogenous loci of the candidate marker genes – *barhl1b* and *eomesa* as seen in Figure 8.1 and 8.2. *eomesa* was highly expressed in the forebrain and *barhl1b* seemed to be expressed in the tectum, as was observed from the colorimetric *in situ* hybridizations.

That the GFP expression was indeed being driven by the integration of QF2 was confirmed by sequencing of the gDNA of the GFP + larvae of *barhl1b:QF2*. The sequence validated that QF2 had been correctly inserted in frame, and was being able to drive GFP expression under the *barhl1b* promoter located upstream (Figure 8.3).

4.4 An intersectional approach to label marker-specific RGCs

Since both marker genes are expressed in multiple regions within the brain, it was important to label marker-specific RGCs alone. The intersectional genetic approach was tested using a pan-neuronal enhancer trap line – *Gal4s1101t* – as the driver, a UAS reporter line, with a membrane bound GFP cassette (GFPcaax) flanked by two *loxP* sites and an *ath5:Cre* line, as shown in Figure 9.1. The intersectional approach was successful, allowing us to visualize RFP-labeled RGCs in a population of neurons labeled by GFP, as seen in Figure 9.2.The same approach was then used with the candidate marker gene-specific driver lines – *barhl1b:QF2* and *eomesa:QF2*.

4.4 *barhl1b* appears to label a discrete population of RGCs

barhl1b, expressed by cells in Cluster 10 of the t-SNE plot (Figure 10.1) appeared to label RGCs that innervated one of the more dorsal layers of the tectum, perhaps the SFGS (Figure 10.2). Staining performed on fixed larvae enabled the analysis of morphology of the labeled RGCs (Figure 10.3). Both DAPI and GFP are false colored in red and cyan respectively, with DAPI being used to gauge the depth of the IPL to study the stratification level of the dendrites of the GFP labeled RGCs.

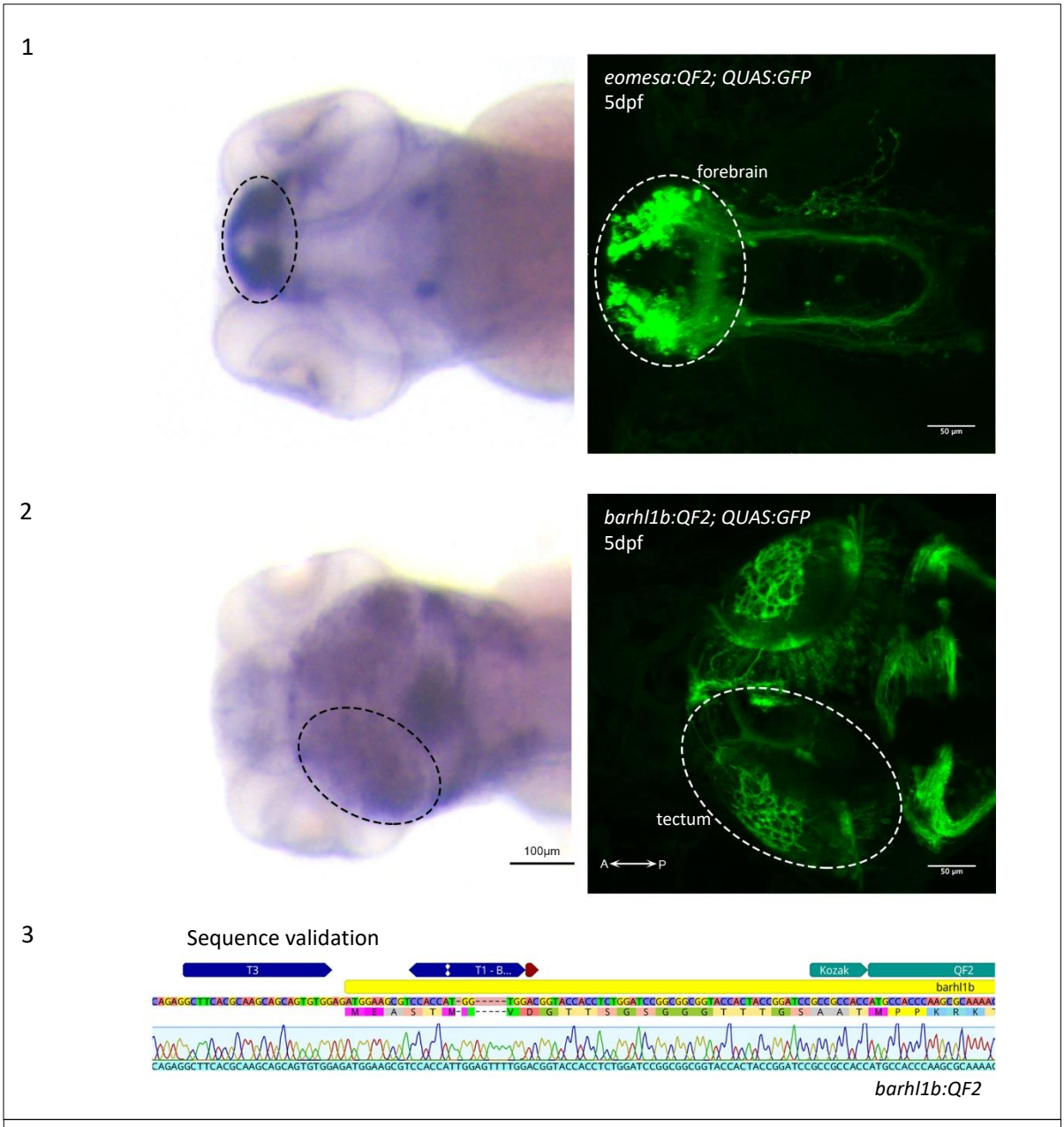

Figure 8: Transient gene expression pattern reflects endogenous expression patterns of candidate marker genes. 1) *eomesa* is highly expressed in the forebrain 2) *barhl1b* is expressed in the tectum 3) Sequence validation of the *barhl1b:QF2* larvae that were GFP + confirms successful and in-frame integration of QF2 at the endogenous marker loci, so as to be able to drive GFP expression under the *barhl1b* promoter, located upstream.

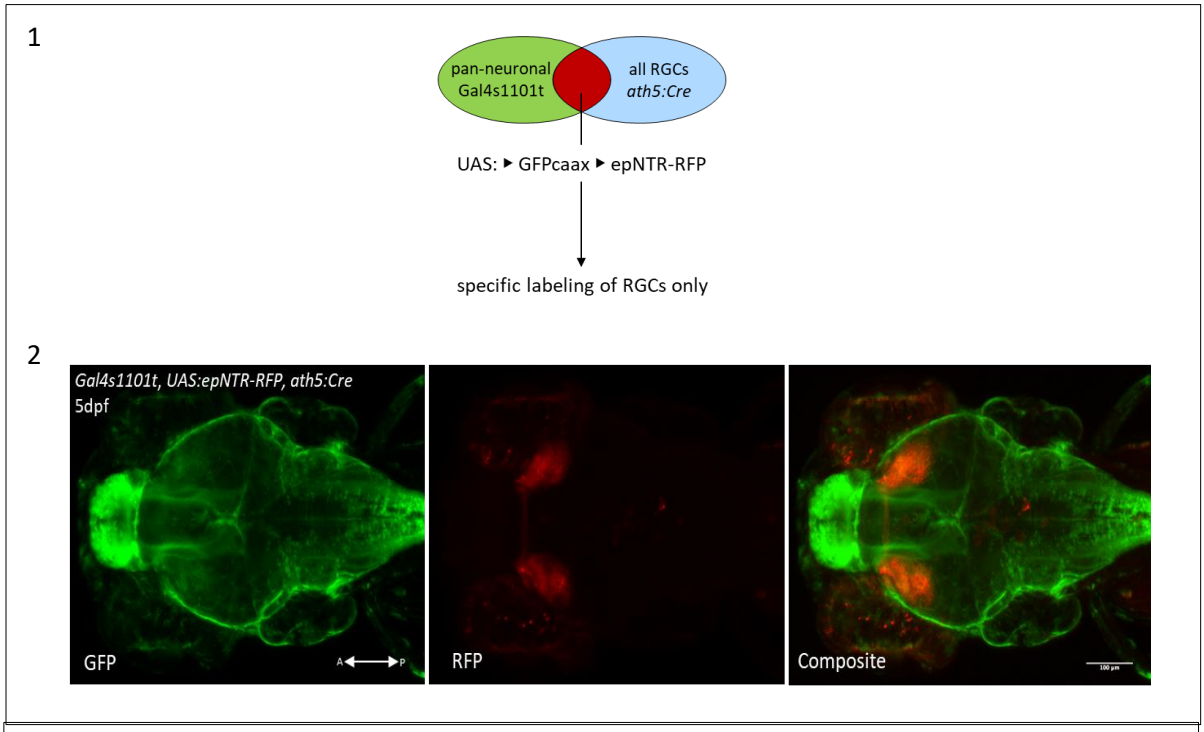

Figure 9: An intersectional approach with *ath5:Cre* mediating recombination only in RGCs. 1) Intersectional genetics schematic with a pan-neuronal driver line, a reporter line with a GFP cassette flanked by two *loxP* sites and *ath5:Cre* line. 2) RFP-labeled RGCs in a population of GFP-labeled neurons could be visualized as seen in the composite image.

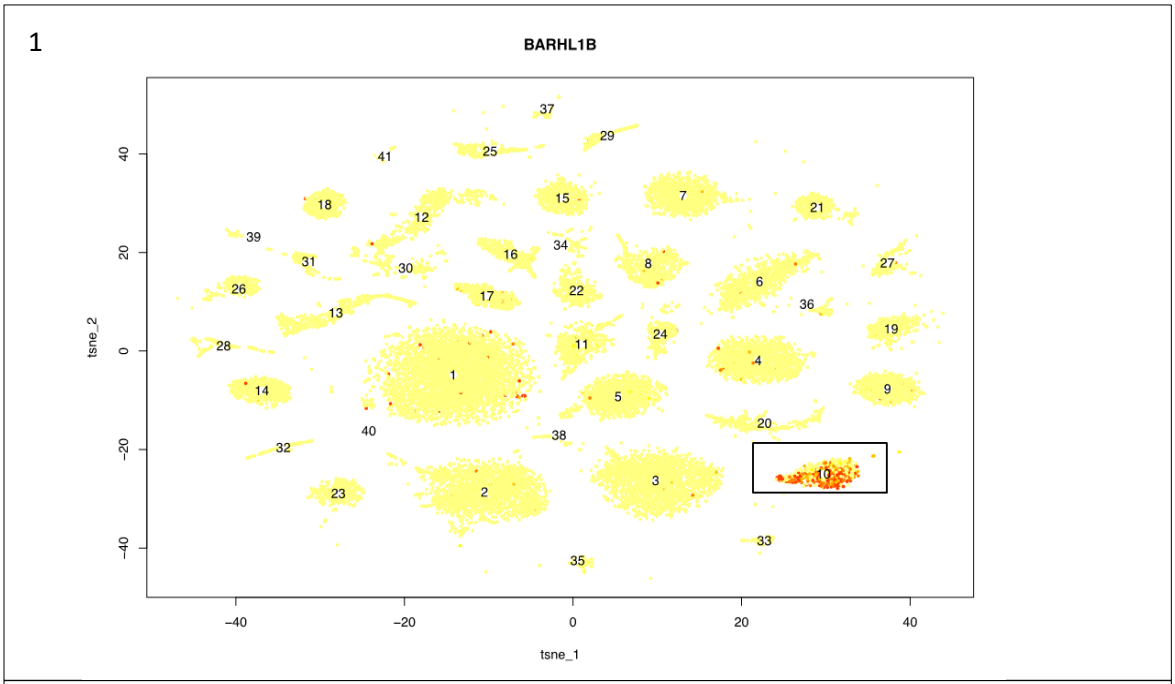

Figure 10: *barhl1b* appears to label a discrete population of RGCs. 1) *barhl1b* expressing cells are observed in Cluster 10 of the t-SNE plot

The plot in Figure 10.4 shows the thickness of the IPL in terms of the DAPI labeling which peaks at the beginning of the GCL and then drops along the IPL where the dendrites stratify – as seen by the two green peaks, only to peak again at the beginning of the INL.

As can be seen from Figures 10.3 and 10.4, *barhl1b* appears to label RGCs that stratify in two layers of the IPL. However, since there are four RGC cell bodies, that appear to be stratifying in the IPL, we cannot state that all four RGCs are in fact, bistratified. They may be bistratified, or a combination of monostratified/bistratified RGCs or RGCs with monostratifications in different sublaminae of the IPL. Thus more rounds of staining performed on larvae with a more sparse expression patterns may help resolve the stratification patterns of the RGC dendritic morphologies.

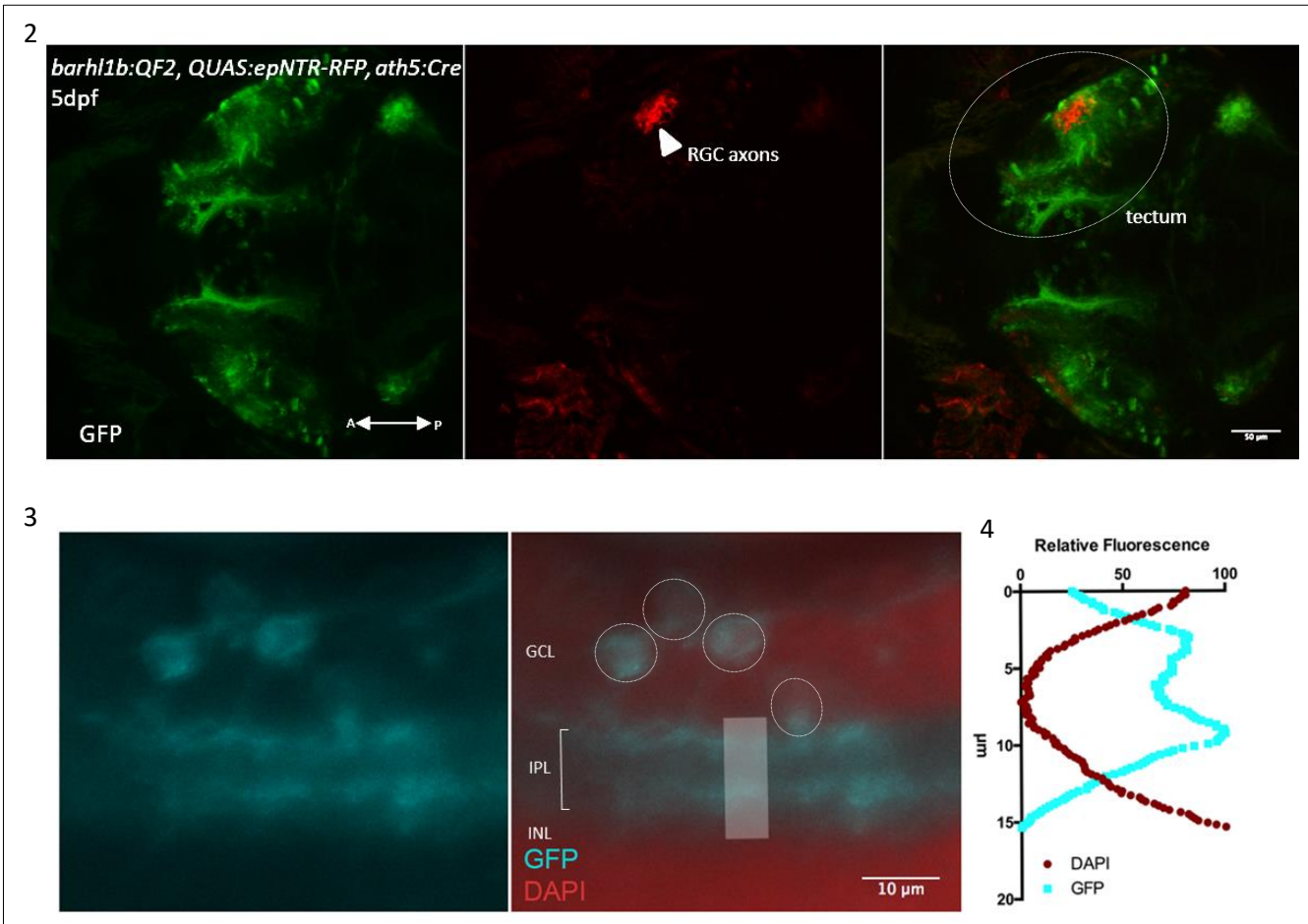

Figure 10: *barhl1b* appears to label a discrete population of RGCs. 2) *barhl1b* + RGCs, labeled with RFP in a population of GFP labeled cells that express *barhl1b*, appear to innervate the dorsal sublaminae of the optic tectum. 3) Analysis of the morphology of the *barhl1b* + RGCs, indicates that they may be bistratified, or a combination of different dendritic stratification patterns

4.4 *eomesa* appears to label a distinct visual pathway

eomesa, broadly expressed in Cluster 28 of the t-SNE plot (Figure 11.1) appeared to label RGCs whose axons projected to AF9 (Figure 11.2).

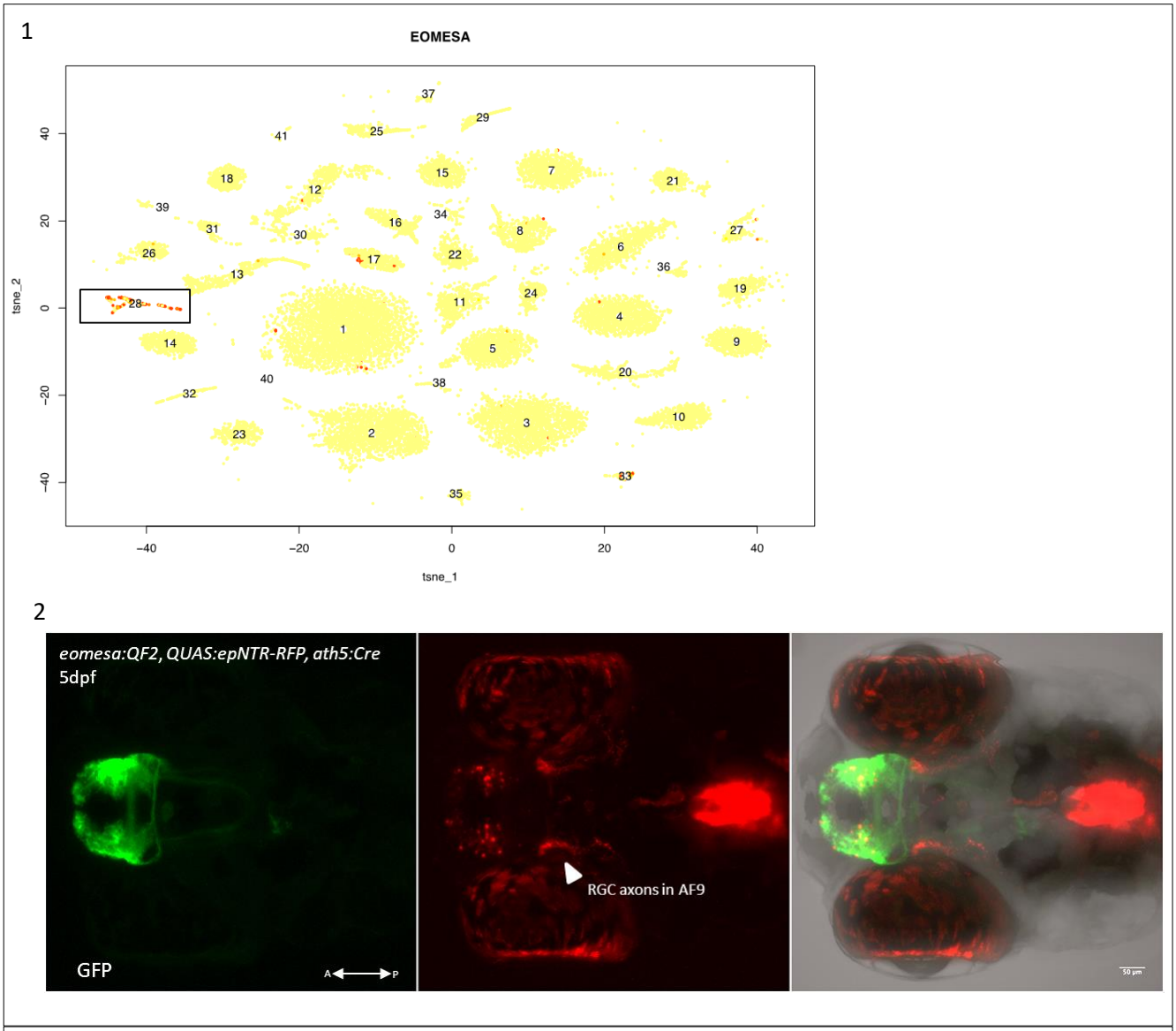

Figure 11: *eomesa* appears to label a distinct visual pathway. 1) *eomesa* expressing cells are observed in Cluster 28 of the t-SNE plot 2) eomesa + RGC axons appear to innervate AF9

CHAPTER FIVE: DISCUSSION

This study presents a transgenic method to map molecular markers onto morphologically classified RGC types. RGCs exhibit tremendous diversity in morphology in terms of dendritic stratification and axonal projection patterns [20]. The prevalence of these projection classes that innervate multiple visual brain areas in indicative of their prominent role in the parallel processing of visual information that generates various, complex visual behaviors. There are also genetic programs that ensure a type-specific innervation of each retinorecipient area, generating retinotopically biased visual maps in the brain [41]. These morphologically diverse classes appear to serve specific functions and therefore it is crucial to access and manipulate them, in a systematic and type-specific manner [2].

Molecular differences arising in these morphologically diverse RGCs can be exploited for gaining genetic access to specific RGC types. High-throughput single-cell RNA-sequencing of ~22,600 RGCs was able to reveal 41 potential markers for RGC types. Of these markers, 2 were validated as markers for RGC types. One was *barhl1b*, enriched in cluster 10, which appeared to label RGCs that innervated the SFGS layer in the optic tectum [42]. However, the morphological analysis revealed that better resolution was required to be able to define the morphology of the RGCs. Another way to study the RGCs in a marker-specific way would be to combine fluorescent *in situ* hybridizations with sparse RGC labeling using variegated lines such as the BGUG, in conjugation with pan-RGC labeling line. Combining this technique with immunohistochemical staining could in principle, enable us to visualize a single RGC with a well-defined dendritic morphology, projecting into a visual brain area in the contralateral tectum.

The other marker under investigation – *eomesa* was broadly expressed in cluster 28. Courtesy unpublished data from the collaboration between the Baier and Sanes lab, we know that the same cluster also contains cells that express another potential marker – *tbx20*. What is truly intriguing about this marker is that it labels a single type of RGC very robustly. This RGC has a specific dendritic morphology and a specific axonal projection pattern that terminates at AF9, which is expressed unwaveringly in all RGCs marked by *tbx20.* From the present study, we know that *eomesa* also marks RGCs that innervate AF9. This sets up a platform for a few interesting propositions. Primarily, it could mean that instead of being a single-type marker like *tbx20, eomesa* could actually be a multi-type marker, labeling RGCs that terminate at

AF9, and also those which terminate at the optic tectum via AF9. This could be resolved by increasing the sample size of the RGCs that are subjected to high-throughput scRNA-seq. Secondly, one could say that RGCs that share transcriptional domains, also may share morphological features, as can be seen from the shared projection patterns of *tbx20* and *eomesa* labeled RGCs.

Thus, the pipeline established in this study to map molecular markers onto morphologically classified RGC types can be used to validate the other candidate markers of RGC types. This will enable the large-scale functional analyses of the multiple, type-specific inputs to visual behaviors. It will also contribute to neuronal cell-type classification efforts by establishing the first degree of connectivity between morphology and molecular composition, along with generating tools for the second degree of connectivity with physiology.

CHAPTER SIX: CONCLUSION AND FUTURE PROSPECTS

CONCLUSIONS:

High-throughput single-cell RNA sequencing data revealed 41 putative markers for morphologically defined RGC types. To gain access to the morphologically defined RGC types, using these candidate markers, transgenesis was established using a homology-independent targeted integration-mediated CRISPR/Cas9 approach. The endogenous expression patterns of the genes were characterized using colorimetric *in situ* hybridizations, for more confident transgenesis. The HITI donor plasmid carrying the driver component of the Q system – QF2, was knocked-in into the endogenous loci of two of candidate marker genes – *barhl1b* and *eomesa*, to drive GFP expression under the promoters of the marker genes. The transient expression pattern matched the endogenous expression patterns, indicating that our transgenic approach was efficient.

The novel driver lines, *barhl1b:QF2* and *eomesa:QF2* were then used in conjunction with an intersectional reporter line, and an *ath5:Cre* line to restrict the expression of the marker genes to RGCs alone. Both markers - *barhl1b* and *eomesa* – appeared to label discrete populations of RGC types. Thus, a transgenic method to map molecular markers onto morphologically classified RGC types was established successfully.

FUTURE PROSPECTS:

Future studies will aim at a functional analysis of RGC types using transgenic lines generated by the approach established here. This will rely on successfully encoding certain tools, such as those of ablations and imaging within the transgenic lines. As a proof of principle and to examine whether the chemogenetic ablation tool – *epNTR* (enhanced potency nitroreductase) being encoded within the intersectional reporter lines was functional, we tested for the ablation RGCs using a pan-RGC line, and performed a visual background adaptation assay (Figure 12.1).

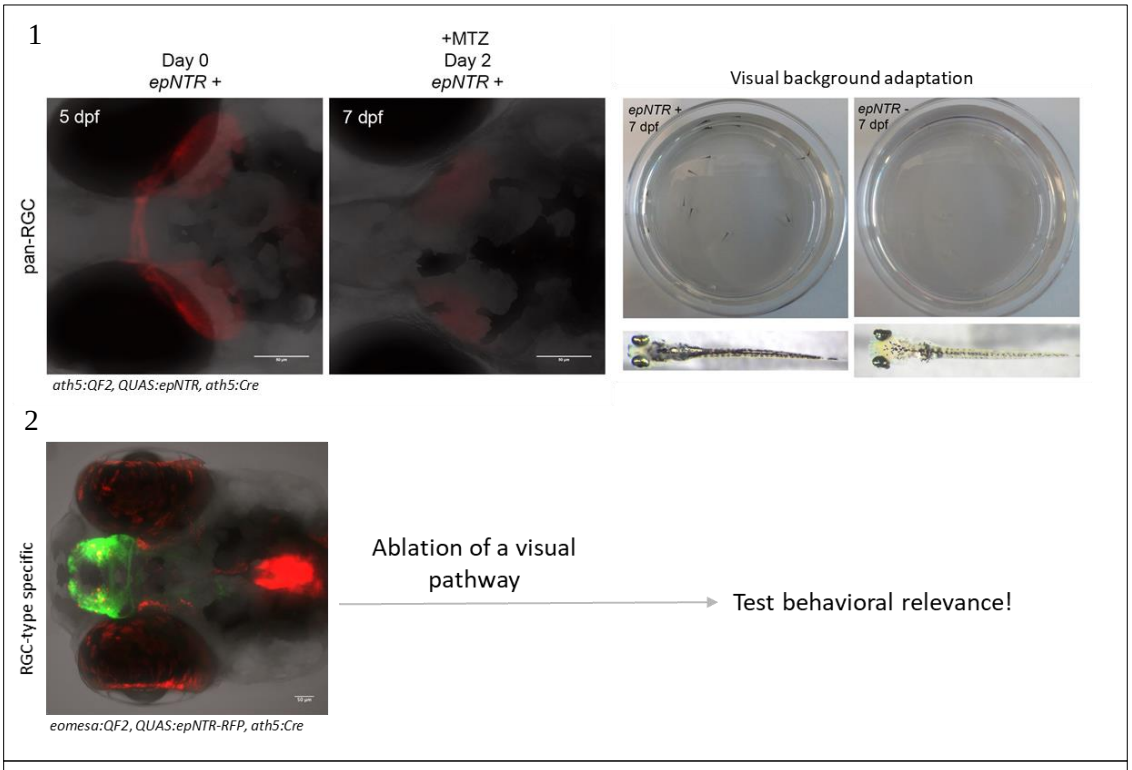

Figure 12: Visual background adaptation assay. 1) *epNTR* + larvae with ablated RGCs, were unable to adapt to the white background, and remained dark, unlike the *epNTR* – larvae which were able to adapt to their visual background, and became pale 2) Future studies will aim at the functional characterization of RGC types using the novel transgenic lines generated by the approach established in this study.

Metrodinazole (MTZ) is a pro-drug that gets converted to a cytotoxic product in the presence of *epTNR*, and thus induces cell death in all cells expressing it. Thus, in this case, all RFP-labeled RGCs carrying *epNTR* were ablated, leading to visual impairment in the larvae.

Visually competent larvae are able to adapt to their visual backgrounds by the rearrangement of melanosomes on their skin in a hormone-mediated reaction. We observed that visually impaired larvae were unable to adapt to their white backgrounds and remained dark, indicating that the RGCs had been successfully ablated and the ablation tool worked.

The same approach could then be used for the ablations of specific visual pathways to test the behavioral relevance of a marker-specific, morphologically classified RGC-type (Figure 12.2). These future studies will of course, require the screening of potential founders to confirm germline transmission which will then give rise to a novel, stable, marker-specific transgenic line.

REFERENCES

[1] H. Zeng, J.R. Sanes, Neuronal cell-type classification: Challenges, opportunities and the path forward, Nat. Rev. Neurosci. 18 (2017) 530–546. doi:10.1038/nrn.2017.85.

[2] E. Robles, The power of projectomes: genetic mosaic labeling in the larval zebrafish brain reveals organizing principles of sensory circuits, J. Neurogenet. 31 (2017) 61–69. doi:10.1080/01677063.2017.1359834.

[3] J.R. Sanes, R.H. Masland, The Types of Retinal Ganglion Cells: Current Status and Implications for Neuronal Classification, Annu. Rev. Neurosci. (2015). doi:10.1146/annurev-neuro-071714-034120.

[4] J. Bilotta, S. Saszik, The zebrafish as a model visual system, Int. J. Devl Neurosci. 19 (2001) 621–629. doi:10.1016/S0736-5748(01)00050-8.

[5] R.W. Friedrich, G.A. Jacobson, P. Zhu, Circuit Neuroscience in Zebrafish, Curr. Biol. 20 (2010) R371–R381. doi:10.1016/j.cub.2010.02.039.

[6] R.W. Friedrich, C. Genoud, A.A. Wanner, Analyzing the structure and function of neuronal circuits in zebrafish, Front. Neural Circuits. 7 (2013) 1–8. doi:10.3389/fncir.2013.00071.

[7] B.J. Melloni, How the retina works., Am. Fam. Physician. 4 (1971) 81. doi:10.1511/2003.1.28.

[8] T. Gollisch, M. Meister, Eye Smarter than Scientists Believed: Neural Computations in Circuits of the Retina, Neuron. 65 (2010) 150–164. doi:10.1016/j.neuron.2009.12.009.

[9] H.S. Seung, U. Sümbül, Neuronal cell types and connectivity: Lessons from the retina, Neuron. 83 (2014) 1262–1272. doi:10.1016/j.neuron.2014.08.054.

[10] Y.A. Pan, T. Freundlich, T.A. Weissman, D. Schoppik, X.C. Wang, S. Zimmerman, B. Ciruna, J.R. Sanes, J.W. Lichtman, A.F. Schier, Zebrabow: multispectral cell labeling for cell tracing and lineage analysis in zebrafish, Development. 140 (2013) 2835–2846. doi:10.1242/dev.094631.

[11] O.S. Dhande, A.D. Huberman, Retinal ganglion cell maps in the brain: Implications

for visual processing, Curr. Opin. Neurobiol. 24 (2014) 133–142. doi:10.1016/j.conb.2013.08.006.

[12] I. Temizer, J.C. Donovan, H. Baier, J.L. Semmelhack, A Visual Pathway for Looming-Evoked Escape in Larval Zebrafish, Curr. Biol. 25 (2015) 1823–1834. doi:10.1016/j.cub.2015.06.002.

[13] J.L. Semmelhack, J.C. Donovan, T.R. Thiele, E. Kuehn, E. Laurell, H. Baier, A dedicated visual pathway for prey detection in larval zebrafish, Elife. 3 (2014) 1–19. doi:10.7554/eLife.04878.

[14] D.G. Gibson, J.I. Glass, C. Lartigue, V.N. Noskov, R.-Y. Chuang, M. a Algire, G. a Benders, M.G. Montague, L. Ma, M.M. Moodie, C. Merryman, S. Vashee, R. Krishnakumar, N. Assad-Garcia, C. Andrews-Pfannkoch, E. a Denisova, L. Young, Z.-Q. Qi, T.H. Segall-Shapiro, C.H. Calvey, P.P. Parmar, C. a Hutchison, H.O. Smith, J.C. Venter, Creation of a bacterial cell controlled by a chemically synthesized genome., Science. 329 (2010) 52–56. doi:10.1126/science.1190719.

[15] H.A. Burgess, H. Schoch, M. Granato, Distinct Retinal Pathways Drive Spatial Orientation Behaviors in Zebrafish Navigation, Curr. Biol. 20 (2010) 381–386. doi:10.1016/j.cub.2010.01.022.

[16] T.C. Badea, J. Nathans, Quantitative analysis of neuronal morphologies in the mouse retina visualized by using a genetically directed reporter, J. Comp. Neurol. (2004). doi:10.1002/cne.20304.

[17] W.I. Mangrum, J.E. Dowling, E.D. Cohen, A morphological classification of ganglion cells in the zebrafish retina, Vis Neurosci. 19 (2002) 767–779.

[18] H. Baier, Synaptic Laminae in the Visual System: Molecular Mechanisms Forming Layers of Perception, Annu. Rev. Cell Dev. Biol. 29 (2013) 385–416. doi:10.1146/annurev-cellbio-101011-155748.

[19] K. Yonehara, B. Roska, Neuroscience: Retinal projectome reveals organizing principles of the visual system, Curr. Biol. 24 (2014) R833–R835. doi:10.1016/j.cub.2014.08.009.

[20] E. Robles, E. Laurell, H. Baier, The retinal projectome reveals brain-area-specific visual representations generated by ganglion cell diversity, Curr. Biol. 24 (2014) 2085–2096. doi:10.1016/j.cub.2014.07.080.

[21] N. Nikolaou, A.S. Lowe, A.S. Walker, F. Abbas, P.R. Hunter, I.D. Thompson, M.P. Meyer, Parametric Functional Maps of Visual Inputs to the Tectum, Neuron. 76 (2012) 317–324. doi:10.1016/j.neuron.2012.08.040.

[22] J.N. Kay, I. De la Huerta, I.-J. Kim, Y. Zhang, M. Yamagata, M.W. Chu, M. Meister, J.R. Sanes, Retinal Ganglion Cells with Distinct Directional Preferences Differ in Molecular Identity, Structure, and Central Projections, J. Neurosci. 31 (2011) 7753–7762. doi:10.1523/JNEUROSCI.0907-11.2011.

[23] D. Förster, I. Arnold-Ammer, E. Laurell, A.J. Barker, A.M. Fernandes, K. Finger-Baier, A. Filosa, T.O. Helmbrecht, Y. Kölsch, E. Kühn, E. Robles, K. Slanchev, T.R. Thiele, H. Baier, F. Kubo, Genetic targeting and anatomical registration of neuronal populations in the zebrafish brain with a new set of BAC transgenic tools, Sci. Rep. (2017). doi:10.1038/s41598-017-04657-x.

[24] E.Z. Macosko, A. Basu, R. Satija, J. Nemesh, K. Shekhar, M. Goldman, I. Tirosh, A.R. Bialas, N. Kamitaki, E.M. Martersteck, J.J. Trombetta, D.A. Weitz, J.R. Sanes, A.K. Shalek, A. Regev, S.A. McCarroll, Highly parallel genome-wide expression profiling of individual cells using nanoliter droplets, Cell. 161 (2015) 1202–1214. doi:10.1016/j.cell.2015.05.002.

[25] A. Mortazavi, B. a Williams, K. McCue, L. Schaeffer, B. Wold, Mapping and quantifying mammalian transcriptomes by RNA-Seq., Nat. Methods. 5 (2008) 621–628. doi:10.1038/nmeth.1226.

[26] K. Shekhar, S.W. Lapan, I.E. Whitney, N.M. Tran, E.Z. Macosko, M. Kowalczyk, X. Adiconis, J.Z. Levin, J. Nemesh, M. Goldman, S.A. McCarroll, C.L. Cepko, A. Regev, J.R. Sanes, Comprehensive Classification of Retinal Bipolar Neurons by Single-Cell Transcriptomics, Cell. 166 (2016) 1308–1323.e30. doi:10.1016/j.cell.2016.07.054.

[27] A.M. Klein, L. Mazutis, I. Akartuna, N. Tallapragada, A. Veres, V. Li, L. Peshkin,

D.A. Weitz, M.W. Kirschner, Droplet barcoding for single-cell transcriptomics applied to embryonic stem cells, Cell. 161 (2015) 1187–1201. doi:10.1016/j.cell.2015.04.044.

[28] C. Thisse, B. Thisse, High-resolution in situ hybridization to whole-mount zebrafish embryos, Nat. Protoc. 3 (2008) 59–69. doi:10.1038/nprot.2007.514.

[29] S. Albadri, F. Del Bene, C. Revenu, Genome editing using CRISPR/Cas9-based knock-in approaches in zebrafish, Methods. 121–122 (2017) 77–85. doi:10.1016/j.ymeth.2017.03.005.

[30] K. Suzuki, Y. Tsunekawa, R. Hernandez-Benitez, J. Wu, J. Zhu, E.J. Kim, F. Hatanaka, M. Yamamoto, T. Araoka, Z. Li, M. Kurita, T. Hishida, M. Li, E. Aizawa, S. Guo, S. Chen, A. Goebl, R.D. Soligalla, J. Qu, T. Jiang, X. Fu, M. Jafari, C.R. Esteban, W.T. Berggren, J. Lajara, E. Nuñez-Delicado, P. Guillen, J.M. Campistol, F. Matsuzaki, G.H. Liu, P. Magistretti, K. Zhang, E.M. Callaway, K. Zhang, J.C.I. Belmonte, In vivo genome editing via CRISPR/Cas9 mediated homology-independent targeted integration, Nature. (2016). doi:10.1038/nature20565.

[31] Y. Kimura, Y. Hisano, A. Kawahara, S.I. Higashijima, Efficient generation of knock-in transgenic zebrafish carrying reporter/driver genes by CRISPR/Cas9-mediated genome engineering, Sci. Rep. 4 (2014) 1–7. doi:10.1038/srep06545.

[32] A. Ghosh, M.E. Halpern, Transcriptional regulation using the Q system in transgenic zebrafish, Methods Cell Biol. 135 (2016) 205–218. doi:10.1016/BS.MCB.2016.05.001.

[33] D.L. Rousso, M. Qiao, R.D. Kagan, M. Yamagata, R.D. Palmiter, J.R. Sanes, Two Pairs of ON and OFF Retinal Ganglion Cells Are Defined by Intersectional Patterns of Transcription Factor Expression, Cell Rep. 15 (2016) 1930–1944. doi:10.1016/j.celrep.2016.04.069.

[34] L. Madisen, A.R. Garner, D. Shimaoka, A.S. Chuong, N.C. Klapoetke, L. Li, A. van der Bourg, Y. Niino, L. Egolf, C. Monetti, H. Gu, M. Mills, A. Cheng, B. Tasic, T.N. Nguyen, S.M. Sunkin, A. Benucci, A. Nagy, A. Miyawaki, F. Helmchen, R.M.

Empson, T. Knöpfel, E.S. Boyden, R.C. Reid, M. Carandini, H. Zeng, Transgenic mice for intersectional targeting of neural sensors and effectors with high specificity and performance, Neuron. 85 (2015) 942–958. doi:10.1016/j.neuron.2015.02.022.

[35] D. Förster, M. Dal Maschio, E. Laurell, H. Baier, An optogenetic toolbox for unbiased discovery of functionally connected cells in neural circuits, Nat. Commun. 8 (2017). doi:10.1038/s41467-017-00160-z.

[36] R. Portugues, F. Engert, The neural basis of visual behaviors in the larval zebrafish, Curr. Opin. Neurobiol. 19 (2009) 644–647. doi:10.1016/j.conb.2009.10.007.

[37] M.B. Orger, E. Gahtan, A. Muto, P. Page-mccaw, M.C. Smear, Behavioral screening assays in zebrafish- Orger 2004.pdf, 77 (2004) 53–68.

[38] H. Baier, E.K. Scott, Genetic and optical targeting of neural circuits and behavior - zebrafish in the spotlight, Curr. Opin. Neurobiol. 19 (2009) 553–560. doi:10.1016/j.conb.2009.08.001.

[39] M. Stemmer, T. Thumberger, M. Del Sol Keyer, J. Wittbrodt, J.L. Mateo, CCTop: An intuitive, flexible and reliable CRISPR/Cas9 target prediction tool, PLoS One. 10 (2015) 1–11. doi:10.1371/journal.pone.0124633.

[40] S. Kirchmaier, K. Lust, J. Wittbrodt, Golden GATEway Cloning – A Combinatorial Approach to Generate Fusion and Recombination Constructs, PLoS One. 8 (2013). doi:10.1371/journal.pone.0076117.

[41] L.M. Nevin, M.R. Taylor, H. Baier, Hardwiring of fine synaptic layers in the zebrafish visual pathway, Neural Dev. 3 (2008) 36. doi:10.1186/1749-8104-3-36.

[42] J.P. Gabriel, C.A. Trivedi, C.M. Maurer, S. Ryu, J.H. Bollmann, Layer-Specific Targeting of Direction-Selective Neurons in the Zebrafish Optic Tectum, Neuron. 76 (2012) 1147–1160. doi:10.1016/j.neuron.2012.12.003.

APPENDIX

To check the efficiency of different Cas9 protein/gRNA complex concentrations in the HITI-mediated CRISPR/Cas9 approach, the following conditions were evaluated using the same protocol as described in Chapter 3.10 and 3.11

RNP Concentration (in µM)	tracrRNA (in µl)	crRNA (in µl)	Duplex Buffer (in µl)	Cas9 (in µl)	Cas9 Working buffer (in µl)
0.75	0.25	0.25	15.5	0.25	9.75
1.5	0.5	0.5	15	0.5	9.5
3.0	1	1	14	1	9
6.0	2	2	12	2	8

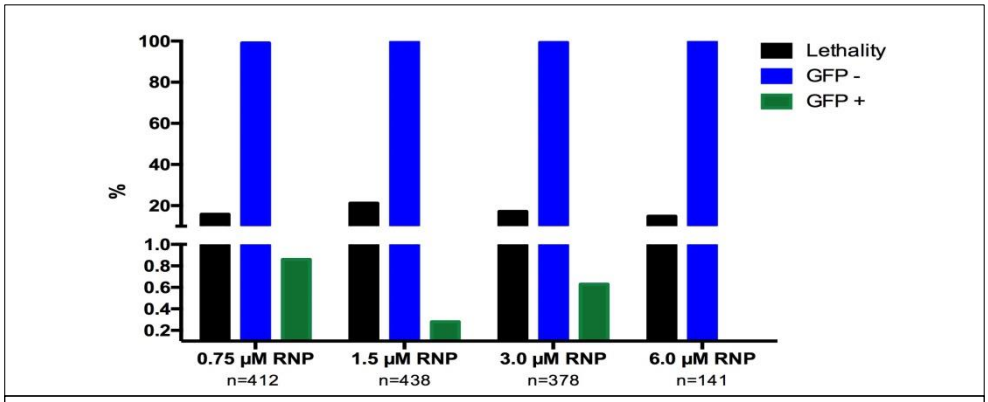

Knock-in efficiencies of different RNP concentrations tested for *barhl1b*

As shown in the figure, concentrations within 0.75µM to 3µM showed no significant differences in efficiency of driving GFP expression from the endogenous marker gene locus. Higher RNP concentrations such as 6µM had zero efficiency. Since the differences were not significant, we decided to use the commonly used concentration that offers high efficiency of driving transient GFP expression, i.e., 1.5µM RNP.